

## **Phased Array Ultrasound System for Planar Flow Mapping in Liquid Metals**

Mäder, K.; Nauber, R.; Galindo, V.; Beyer, H.; Büttner, L.; Eckert, S.; Czarske, J.;

Originally published:

April 2017

**IEEE Transactions on Ultrasonics, Ferroelectrics and Frequency Control 64(2017)9,  
1327-1335**

DOI: <https://doi.org/10.1109/TUFFC.2017.2693920>

Perma-Link to Publication Repository of HZDR:

<https://www.hzdr.de/publications/Publ-24498>

Release of the secondary publication  
on the basis of the German Copyright Law § 38 Section 4.

# Modular Phased Array Ultrasound Velocimeter for 2d-2c Flow Mapping in Liquid Metals

Kevin Mäder, Richard Nauber, Vladimir Galindo, Hannes Beyer, Lars Büttner, Sven Eckert, Jürgen Czarske

**Abstract**—Research in magnetohydrodynamics (MHD) aims at a better understanding of the interaction of conductive fluids and time-varying magnetic fields. Controllable magnetic fields can be used to optimize flows in technical and industrial processes involving liquid metals in order to improve quality and yield. However, necessary experimental studies for the investigations on physical models at room temperature are often limited by the performance of flow instrumentation for opaque liquids. With the phased array ultrasound Doppler velocimeter (PAUDV) we present a modular research platform for flow mapping in liquid metals. It consists of a modular electronics unit capable to interface ultrasound arrays with up to 256 channels. Each channel can be individually configured regarding the excitation pattern (three-level quantization, 64 samples) and the delay (1.6 ns resolution). With the individual addressing of channels the phased array technique to dynamically focus the ultrasound beam can be employed. This allows to resolve smaller flow structures in planar measurements compared to fixed-beam sensors. In addition, it enables the use of receive beamforming and plane wave transmission, which allows to significantly increase the time resolution and to perform 2d flow mapping with only one acoustical access via the cross beam technique. Fast electrical traversing of the measurement volume allows to obtain and visualize turbulence statistics. The capabilities of this research platform are demonstrated on measurements in the alloy gallium-indium-tin at room temperature. 2d velocity measurements of a flow in a cubic vessel influenced by a rotating magnetic field (RMF) are shown and compared to results of a semi-analytical simulation. Furthermore, two-point correlation functions of the velocity field for different magnitudes of the RMF are presented and discussed.

## I. INTRODUCTION

In magnetohydrodynamics (MHD), the interaction between conductive fluids and time-varying magnetic fields is investigated. A better knowledge of this complex interaction can improve the control of melt flows by custom magnetic fields. This can be used to optimize technical and industrial processes involving liquid metals regarding the quality of the product or the yield of the process: For instance, the quality of steel slabs can be improved [1] or the production process for solar cells can be made more energy-efficient [2] using magnetic fields for melt flow shaping. Furthermore, the performance of redox flow batteries using zinc-electrolyte slurry [3] may be improved by magnetically controlled flow of the fluid electrolyte.

K. Mäder, R. Nauber, H. Beyer, L. Büttner and J. Czarske are with the Laboratory of Measurement and Sensor System Techniques (MST), TU Dresden, 01062 Dresden, Germany, e-mail: kevin.maeder@tu-dresden.de.

V. Galindo and S. Eckert are with the Helmholtz-Zentrum Dresden-Rossendorf (HZDR), Bautzner Landstrasse 400, 01328 Dresden, Germany.

Manuscript received xxxxx, xxxxx.

Research in MHD relies on both simulations and model experiments. The latter is important in order to validate results of simulations and especially to investigate turbulent flows, where simulations are often limited by their high computational effort. In laboratory-scale model experiments, electrically conductive alloys with a low melting point that allow experiments at room temperature like gallium-indium-tin (GaInSn) are used [4]. However, the experimental output is limited by the performance of flow instrumentation for opaque liquids. Ultrasound Doppler velocimetry allows spatially resolved velocity measurements in liquid metals [5]. Typical MHD experiments investigating small-scale and turbulent flows often require a spatial resolution in the low millimeter range. With arrays consisting of non-focussing single element transducers that don't allow dynamic sound field shaping, the spatial resolution in the lateral direction along the measurement lines is limited by the divergence of the far field ultrasound beam. With such systems only best case spatial resolutions of approx. 3 mm [6], [7] can be achieved. With the application of the phased array principle however the sound pressure field can be dynamically focussed and traversed in the measurement plane [8], in order to achieve the desired spatial resolution.

In this paper, we present the phased array ultrasound Doppler velocimeter (PAUDV) as a modular ultrasound flow measurement system that provides a generic and extensible platform for model experiments in MHD. It combines the ultrasound Doppler velocimetry principle with an adaptive sound field by transmit- and receive-side beamforming. The PAUDV is flexible regarding the experimental setup and it allows for example two-component, two-dimensional (2d-2c) flow mapping with one-sided acoustical access. This is demonstrated in this paper by measurements in a cubic vessel filled with GaInSn under the influence of a rotating magnetic field (RMF). Further measurement modalities can be obtained by the PAUDV, for instance two-point correlation functions.

## II. PHASED ARRAY ULTRASOUND DOPPLER VELOCIMETER (PAUDV)

### A. Hardware

The PAUDV is a flexible measurement system designed to be used in a wide range of model experiments in MHD. It employs a modular architecture as shown in Fig. 1, which is scalable to drive up to 256 individual channels simultaneously with the specifications given in Table I. The main hardware unit is housed in a standard 19 inch rack-mountable chassis. It can contain up to eight transceiver modules supporting 32 channels each. Each module contains transmit (TX)

TABLE I: Specifications of the PAUDV

| Transmit Path              |  |
|----------------------------|--|
| individual channels        | 256                                    |
| excitation voltage         | $U_{\max} = 200 \text{ V}$             |
| frequency                  | $1 \text{ MHz} < f_0 < 10 \text{ MHz}$ |
| burst pattern              | 64 samples, 3 level quantization       |
| time delay resolution      | $\Delta t = 1.6 \text{ ns}$            |
| max. pulse repetition rate | $f_{\text{PR},\max} = 20 \text{ kHz}$  |
| Receive Path               |  |
| static RX gain             | 17 ... 67 dB                           |
| time-dependent gain        | -5 ... 31 dB                           |
| A/D quantization           | 12 bit                                 |

TABLE II: Specifications of the linear phased array probes

| array number                      | 1          | 2            |
|-----------------------------------|------------|--------------|
| number of elements $n$            | 128        | 128          |
| element pitch $\Delta x$          | 0.5 mm     | 0.3 mm       |
| element height $h$                | 5 mm       | 3 mm         |
| nominal center frequency $f$      | 3.1 MHz    | 3.8 MHz      |
| bandwidth $f_{\text{bw}}$ (-6 dB) | 1.4 MHz    | 2.4 MHz      |
| manufacturer                      | SONAXIS SA | IMASONIC SAS |

beamformers, three-level pulsers, transmit-receive switches and receive (RX) amplification stages. The amplification can be configured regarding a static gain and a time-dependent gain curve to compensate for ultrasound attenuation. The transducer arrays are connected to the transceiver modules by an exchangeable analog signal backplane. This allows to adapt to different probe interfaces and element mappings.

The overall orchestration and parametrization of the transceiver modules is conducted by a controller module that communicates over a control backplane. It utilizes a 32 bit microcontroller (ATSAM4SA16C, Atmel, San Jose, USA) with a stabilized clock source that acts as a common timebase for the PAUDV. The amplified ultrasound echo signals are digitized in the acquisition modules, consisting of an 32 channel A/D-converter (NI 5752) and an FPGA (NI PXIe 7965, National Instruments, Austin, USA). Depending on the number of A/D-converters  $n_{\text{A/D}}$ ,  $32 \cdot n_{\text{A/D}}$  elements can be used on the receive side. The RX-elements can be chosen freely in groups of 16 elements.

For the measurements two ultrasound custom made linear phased arrays were used. The specifications of both arrays are listed in table II.

### B. Control Software

The control software of the PAUDV consists of two parts: the host software implemented in the programming language Python [9] and the firmware of the controller module. The experiment to conduct is described on a high level using the host software: The experimental procedure, all parameter settings, needed environment are described by an experimental setup and a hierarchical set of measurement tasks. The experimental setup includes a model of the measurement setup

which includes geometric (sensor geometry and placement) and acoustical properties (sound speed, density). The object-oriented representation of the measurement procedure allows a wide range of experiments to be specified in a structured manner. A variety of parameters like composition of transmit and receive subapertures, excitation patterns or pulse repetition frequency can be configured individually for each task. In order to execute a described experiment, the host software generates an intermediate representation of the experimental sequence, which is translated to bytecode and transferred to the controller module. In addition, any experimental setup can be used to run acoustical simulations of the specified experiment. The simulation software is based on the open-source tool “efit 2d” [10].

The controller module ensures a deterministic execution of the intermediate program, which allows to control time-critical functionality and parametrize the transceiver modules in a synchronized way. The controller firmware implements a domain-specific instruction set to provide maximum flexibility regarding different measurement modes.

### C. Signal Processing

The digital signal processing chain of the PAUDV is implemented on the FPGA modules and the host PC. The digitized signals are directly fed from the A/D-converter modules to the FPGAs, which can implement custom preconditioning algorithms such as digital filtering, receive beamforming and I-Q demodulation. The results are transferred via PXIe to the host PC, which performs further signal processing, post processing and flow visualization according to the specified measurement tasks. A parallelized execution of independent computation tasks is supported to improve the runtime performance. In addition, computational intense parts like beamforming are implemented using PyOpenCL [11] which enables acceleration by the efficient usage of CPU and GPU units.

The velocity estimation is performed using the Kasai autocorrelation algorithm [12], [13]: The echo signals are bandpass-filtered, receive-beamformed and I-Q demodulated. Evaluating the autocorrelation function gives an estimation of the Doppler frequency shift due to the movement of scattering particles. Single measurements with a high variance of the Doppler frequency shift [12] are discarded. Two-component (2c) velocity data is provided by a coordinate transform of two velocity values from two different measurement directions using the cross beam technique [14], [15]:

$$\mathbf{v} = (\mathbf{s}_1 \mathbf{s}_1^T + \mathbf{s}_2 \mathbf{s}_2^T)^{-1} (\mathbf{s}_1 v_1 + \mathbf{s}_2 v_2) \quad (1)$$

$$= \mathbf{A}^{-1} (\mathbf{s}_1 v_1 + \mathbf{s}_2 v_2) \quad (2)$$

The different measurement directions here are realized by different receive subapertures (see figure 2. This enables 2d-2c flow mapping in experimental setups where only a single acoustical access is available. As the PAUDV offers an open and easily adaptable control software other flow imaging algorithms [16] can be implemented too.

## III. CHARACTERIZATION

To characterize the PAUDV a measured sound pressure field is compared to results of a 2d efit simulation. For this

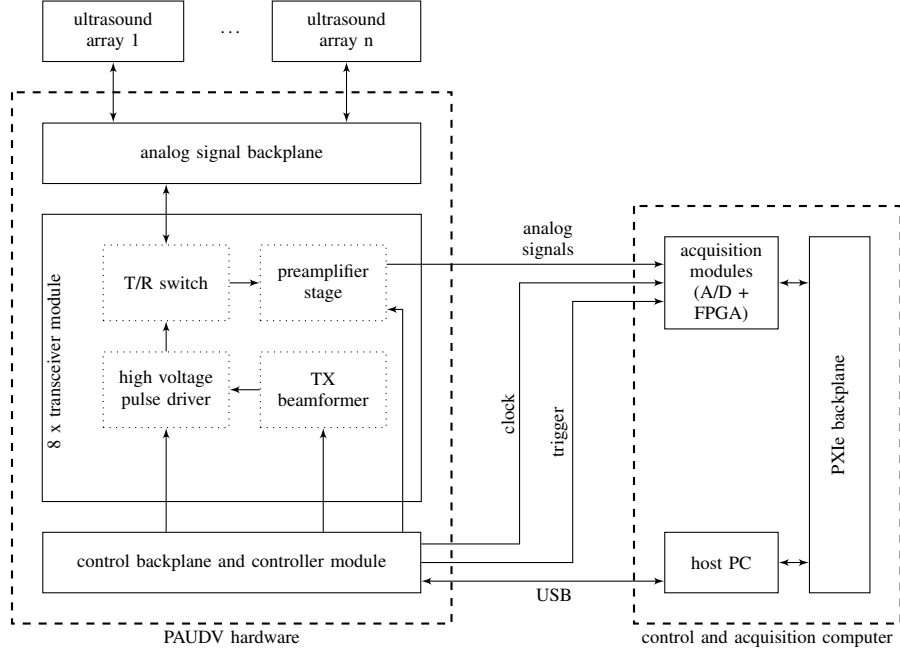


Fig. 1: Architecture of the PAUDV: The main hardware unit consists of up to 8 transceiver modules, a controller module, a control backplane and an analog backplane; High level control and signal acquisition is performed on an embedded host PC.

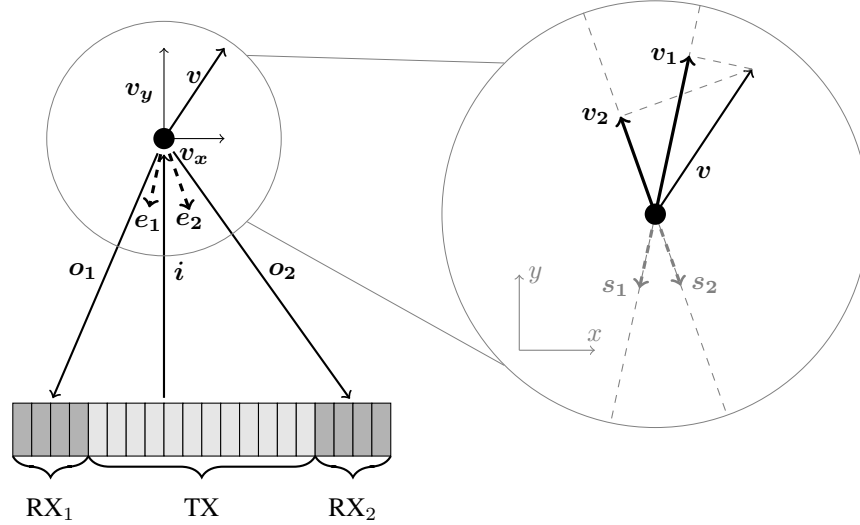


Fig. 2: Cross Beam principle: During transmit the whole ultrasound array is used to send an unsteered plane wave (incident direction  $i$ ). In receive mode the array is partitioned into 2 subapertures  $RX_1$  and  $RX_2$ . These observe a beamforming in the directions  $o_1$  and  $o_2$  respectively. Through the 2 subapertures the projected velocity values  $v_1$  and  $v_2$  ( $v$  projected on the sensitivity directions  $s_1$  and  $s_2$ ) are measured.

experiment ultrasound array 1 (see table II) was used to focus in a bassin filled with water. For the focussing only the 64 elements in the center of the aperture were used. The focus spot was placed on the centerline of the array, 42 mm in front of the array. The emitted ultrasound burst had a frequency of  $f_e = 3$  MHz. The sound pressure field was acquired by moving a scatterer in an area around the focus in the water bassin and recording the echo from the scatterer with one middle element of the phased array. For the scatterer a thin fibre ( $d \approx 70 \mu\text{m}$ ) was used. As the scatterer dimension is

far smaller than the expected focus width the scatterer can be considered as point-like. For positioning it was mounted on a 2d positioning table (repeat accuracy . The plots of the simulated and measured soundfield for this focussing task (see figure 3) show that the actual focus quality with the PAUDV is in good agreement with the expected soundfield given by the simulation. The lateral cross section of the sound fields (see figure 4) show a measured full width at half maximum as a lateral resolution of  $x_{FWHM, \text{meas}} = 0.91 \text{ mm}$ . This is close to the theoretical limit determined by the simulation of

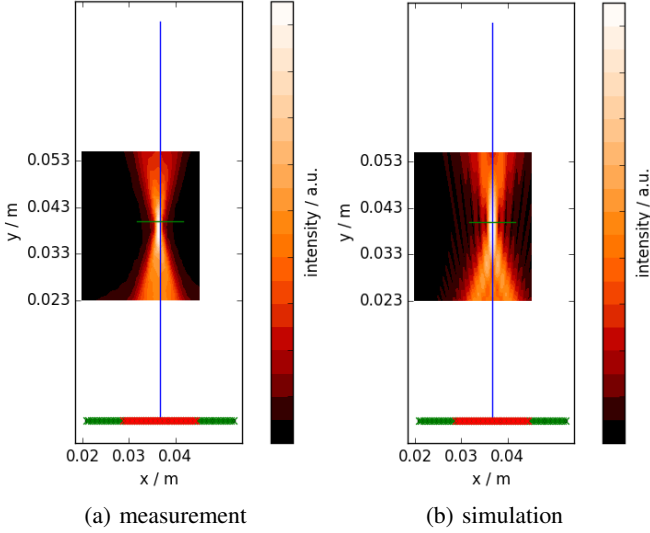


Fig. 3: Soundfield of PAUDV for a focussed point on the centerline of the array in water: Measurement results (a) and results of a efit 2d simulation (b) are shown. The active 64 elements during receive are located in the middle of the array probe.

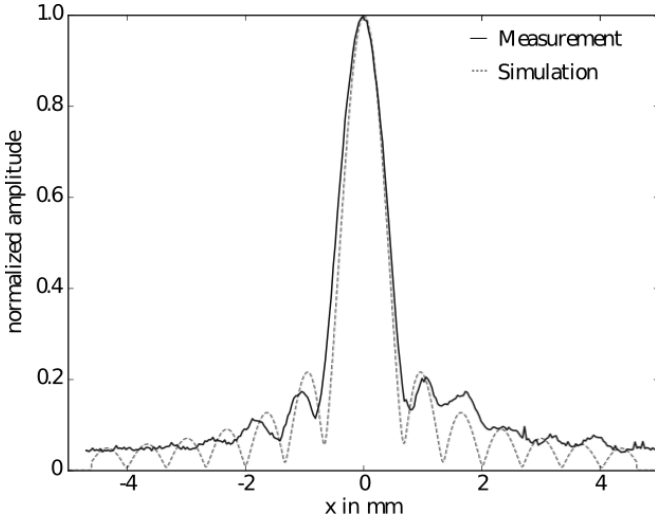


Fig. 4: Lateral cross section through the focus point at  $y = 40$  mm of the simulated and measured soundfields.

$x_{FWHM, sim} = 0.75$  mm, which confirms the functionality of the PAUDV.

#### IV. COMPARISON WITH SIMULATION

To show the performance of the PAUDV, a 2d-2c velocity measurement of a steady flow of GaInSn exposed to an RMF is shown and compared to a simulation. The measurement setup (see figure 5) was chosen as an exemplary object of research in MHD. Investigations of electrically conductive fluids in cylindrical and cubic vessels under the influence of a RMF have been done in previous simulational and partly in experimental studies [17]–[20].

The experiment was conducted in a cube with an inner edge length of  $L = 69$  mm and 6.5 mm thick PMMA walls. The

RMF was rotating around the  $z$ -axis with an angular frequency of  $\omega = 2\pi \cdot 50$  Hz. The magnitude of the RMF was chosen to achieve a laminar flow near the transition to a turbulent flow regime. Measurements were conducted with a RMF rotating in clockwise (cw) or in counterclockwise (ccw) direction. The array probe (ultrasound array 2, see table II) was placed in the central horizontal plane ( $z = 0$ ) on an outside wall of the cube. In the  $x$ -direction, the probe was placed such that its active area was aligned with the inside surface of a side wall of the cube (see figure 5). As a base for comparison, a simulation of the flow in the liquid metal based on a semi-analytic expression of the induced electromagnetic force density was carried out using the open source library OpenFOAM [21].

For transmission, plane waves were formed using all elements of the probe with a pulse repetition frequency  $f_{PR} = 100$  Hz. On the receive side, the probe was partitioned into two subapertures. The apertures contain the outermost 48 elements on each side of the probe. Using the cross beam technique, a 2d-2c velocity field can be obtained from the two one-component (1c) velocity fields of the receive apertures. Velocity estimation was done using the autocorrelator with an ensemble length (number of burst emissions per profile) of  $n_{EPP} = 20$ . For the 1c velocity fields measurement outlier with a high variance of the Doppler frequency shift [12] are discarded. Further, no clutter filter was used in signal processing as the expected velocity field contains velocity vectors perpendicular to the sensitivity directions  $s_i$  of the receive apertures. In these cases, a clutter filter would also filter the whole measurement signal which would lead to artefacts in 1c and resulting 2c velocity fields. The sensitivity directions  $s_i$  are determined by the sending direction vector  $i$  (perpendicular of transmit aperture through the beamforming gate) and the receiving direction vectors  $o_i$  (center point of receive aperture to beamforming gate position) using

$$s_i = \frac{i - o_i}{\|i - o_i\|}. \quad (3)$$

For comparison with the simulation, a measurement consisting of 400 acquired velocity profiles was averaged in time. The region for comparison with the simulation results was chosen to be the first quadrant of the  $x$ - $y$ -plane. Other regions were taken out as these are either notinsonified by the plane wave (second and third quadrant) or show artefacts resulting from multiple wall reflections in the fourth quadrant. Because of the symmetry of the measurement setup the flow field is expected to be symmetric to the  $x$ - and  $y$ -coordinate axes, which makes it feasible to only look at a single quadrant as well.

In figure 6 velocity plots of the measurement and the simulation with a clockwise RMF are presented. As can be seen from the simulation, a clockwise vortex and a counterclockwise vortex in the edge of the cube characterize the steady flow for a clockwise RMF. From the measurement data the expected main clockwise vortex can be clearly recognized. A counterclockwise vortex in the corner of the cube cannot be seen clearly, which might be due to the spatial resolution of measurements with both receive apertures of  $x_{FWHM,1} = 3.5$  mm and  $x_{FWHM,2} = 4.1$  mm respectively.

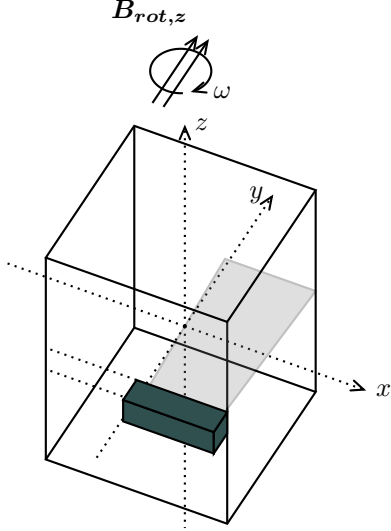


Fig. 5: Measurement setup: A magnetic field  $B_{rot,z}$ , which is rotating around the axis  $z = 0$  is applied around the vertical central axis ( $x = y = 0$ ) of a cube filled with GaInSn. A linear phased array probe is attached in the central horizontal plane ( $z = 0$ -plane). The origin of the coordinate system is at the center of the cube.

The correlation factor of the absolute value of the measured velocity field and the simulation results is 0.91. The correlation factors for the single velocity components  $r_x$  and  $r_y$  are 0.92 and 0.95 respectively.

In addition, on a line  $y = 29$  mm a cross section through the simulated and averaged measured velocity field of the RMF rotating in clockwise direction is taken (see figure 8). For each measured data point the standard deviation is calculated from the 400 velocity profiles available. Error bars denoting a  $1\sigma$  confidence interval are marked on the cross section. For the velocity component in x-direction  $v_x$ , the expected profile from the simulation lies inside the error bars of the measurement. For the velocity component in y-direction  $v_y$ , the expected and measured profiles only agree up to  $x = 29$  mm. Closer to the side wall the velocity is underestimated by the measurement. This effect might be due to the spatial resolution of the measurement system at that point. As the spatial resolution of the two measurements is 2.3 mm and 1.6 mm respectively the velocity field results from averaging over an area around the desired measurement point.

In order to estimate the lateral resolution, sound field simulations using the 2d efit simulation tool of the PAUDV were conducted for both receive apertures. As a worst case approximation, the full width at half maximum (FWHM) for both apertures was calculated near the wall opposite to the array probe (distance of  $d = 68$  mm  $\approx L$  to the probe) as  $\Delta x \approx 3.5$  mm for both apertures. In order to show the performance of the PAUDV system in a different flow structure the flow induced by a counterclockwise rotating RMF was measured, too. Measurement and simulation results for this setup are shown in figure 7.

Additionally to measurement with a constant RMF measure-

ments with a sudden change of direction of the RMF can be conducted. The time-resolved velocity fields of such a reversal of the RMF are shown in [22].

## V. TWO-POINT CORRELATION

Vortices of turbulent flows can be characterized by different length and time scales. Some of these scales, especially the Integral and the Taylor-microscale, can be calculated from experimental velocity field data using two-point correlations of the velocity fluctuations  $v' = v - \bar{v}$  with  $v$  denoting the actual velocity and  $\bar{v}$  the time average [23]. These are cross-correlations  $R_{ij}(\Delta x)$  of velocities  $v_i/v_j$  at positions separated from each other by

$$\Delta x = r \cdot e_{corr} \quad (4)$$

with the correlation line vector  $e_{corr}$  and the distance  $r$ . The two-point correlation  $R_{ij}$  can be calculated as follows

$$R_{ij}(\Delta x) = \frac{1}{T} \int_0^T (v_i(x_0, t) - \bar{v}_i) \cdot (v_j(x_0 + \Delta x, t) - \bar{v}_j) dt \quad (5)$$

$$= \frac{1}{T} \int_0^T v'_i(x_0, t) \cdot v'_j(x_0 + \Delta x, t) dt \quad (6)$$

while  $v_i$  and  $v_j$  are profiles of duration  $T$  of the velocity components  $i$  or  $j$  and at the positions  $x_0$  and  $x_0 + \Delta x$  respectively.

Two often referenced types of two-point correlations are denoted as f- and g-correlation: For the f-correlation the common base vector  $e_i = e_j$  for the velocity profiles  $v_i/v_j$  and the correlation line vector  $e_{corr}$  are parallel to each other.

$$f = R_{ii}(r \cdot e_i) / R_{yy}(0) \quad (7)$$

In contrast the g-correlation specifies two-point correlations where the base vector for the velocity profiles is orthogonal to the correlation line vector  $e_{corr}$ :

$$g = R_{ii}(r \cdot e_j) / R_{yy}(0) \quad (8)$$

$$\text{with} \quad (9)$$

$$e_i \perp e_j \quad (10)$$

For the specified experiment the flow of GaInSn in the cube was observed for a rotating magnetic field with 4 different field densities  $B_{rot,z}$  in order to observe the shift from a laminar to a near-turbulent flow regime in the cube. The f- (figure 9a) and g-correlation (figure 9b) were calculated for the point  $p = (31 \text{ mm}, 0, 0)$  close to the center of a side wall of the cube for the y-component of the velocity field. For both the f- and g-correlation it is notable that the correlation coefficient is higher for larger magnetic field values  $B_{rot,z}$  for equal values of the distance  $r$ . This could be explained with the increasing influence of velocity fluctuations caused by the transition from the laminar to a turbulent flow. For low magnetic fields  $B_{rot,z} = 0.33 \text{ mT}$  a laminar flow regime is present in the cube. Therefore the fluctuations are mainly due to noise induced by the measurement system. As this is

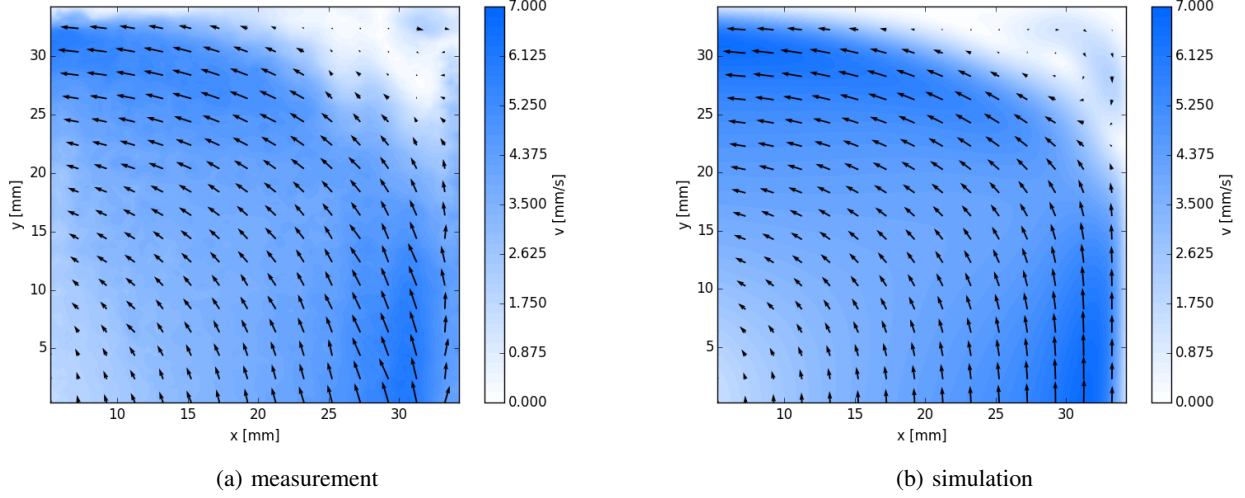


Fig. 6: Measured velocity field (a) and simulation result (b) of the flow velocity in a quarter of the central plane of the cube resulting from a RMF ( $B = 0.33$  mT) rotating in clockwise direction.

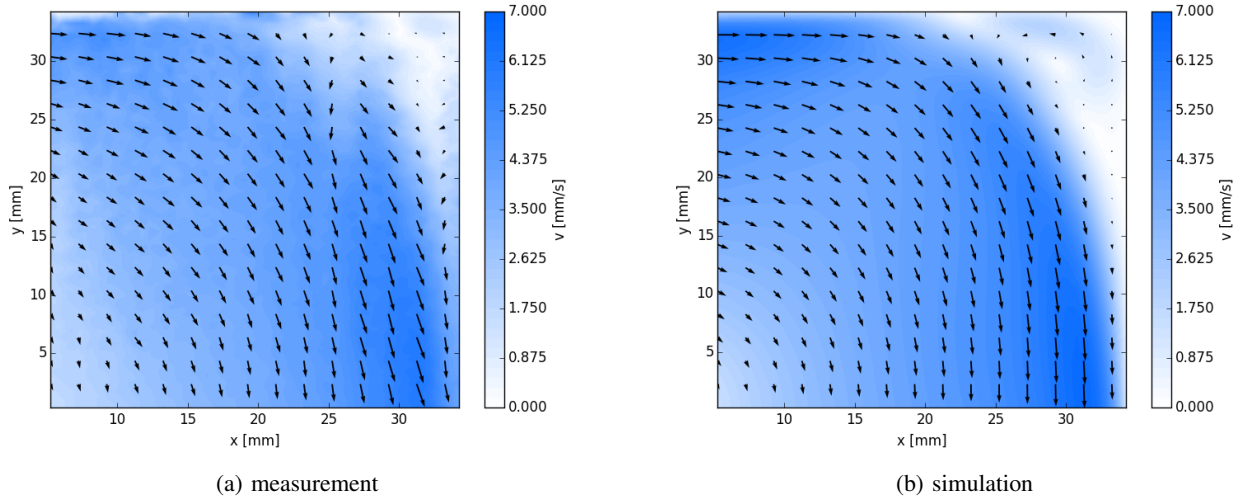


Fig. 7: Measured velocity field (a) and simulation result (b) of the flow velocity in a quarter of the central plane of the cube resulting from a RMF ( $B = 0.33$  mT) rotating in counterclockwise direction.

uncorrelated for different times and positions a steep decrease of the correlation coefficient can be expected. For increasing magnetic fields  $B_{rot,z}$  the flow tends to a shift from the laminar to a turbulent regime thus resulting in fluctuations caused by the flow regime transition. As these fluctuations propagate in the flow an increase of the correlation coefficient can be noted.

## VI. CONCLUSION AND OUTLOOK

The PAUDV is a modular measurement platform for velocity measurements in opaque liquids. Through the combination of the pulse wave ultrasound Doppler principle with the phased array technique it allows 2-component, 2-dimensional flow mapping using an adaptive sound field. Compared to fixed-beam systems the dynamic focussing of the sound field allows higher spatial resolutions close to the theoretical maximum

imposed by the Abbe limit. In this paper we demonstrated the capabilities of the PAUDV through flow mapping of liquid metal in a cube. For the first time the 2d-2c flow was measured with only a single acoustical access. The measurement was performed with a temporal resolution of  $\Delta t = 200$  ms and was in good agreement with a velocity field obtained by a simulation of the flow. By utilizing an adaptive sound field, a lateral resolution of 3.5 mm at a distance of 68 mm from the transducer is shown for the given setup in GaInSn. Because of the high spatial resolution it was feasible to calculate two-point correlation from the measured velocity fields, which can be used to characterize the flow regime. With the flexibility of the PAUDV regarding the measurement modalities and the experimental setup, the measurement system can be easily adapted to different experiments. It is planned to apply the PAUDV system to further laboratory-scale model experiments

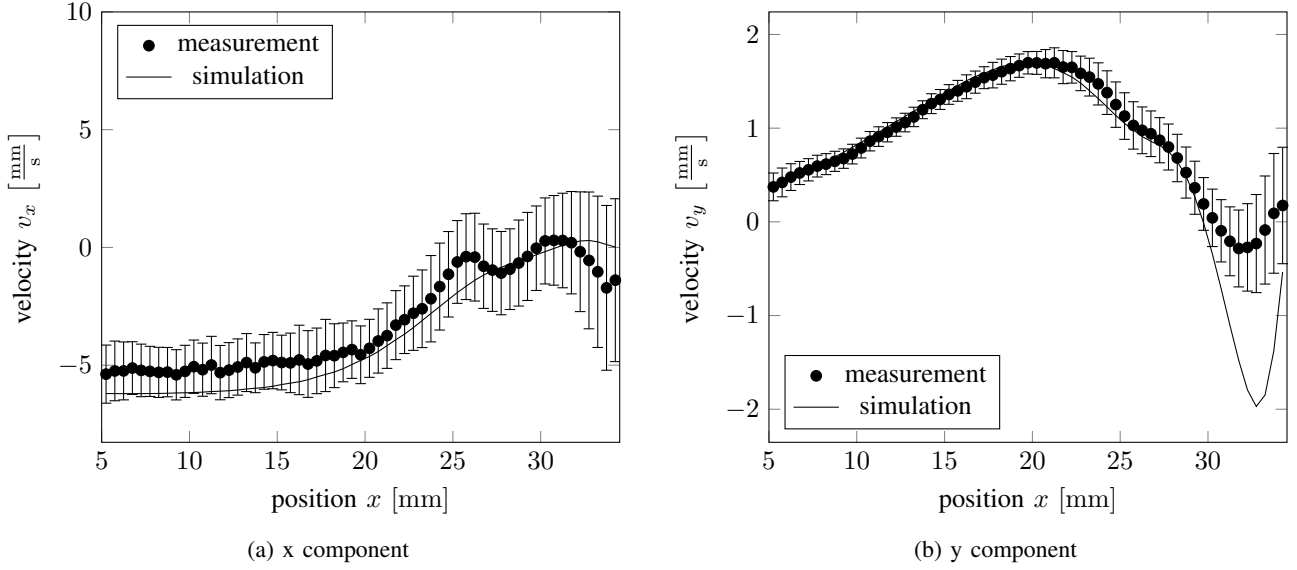


Fig. 8: Cross section of the measured velocity field and simulational result along the line  $y = 29$  mm in the center horizontal plane of the cube. The RMF ( $B = 0.33$  mT) was rotating in clockwise direction. The plots show cross sections of the x component (a) and y component (b) respectively. The error bars show the  $1\sigma$  error of the measurement.

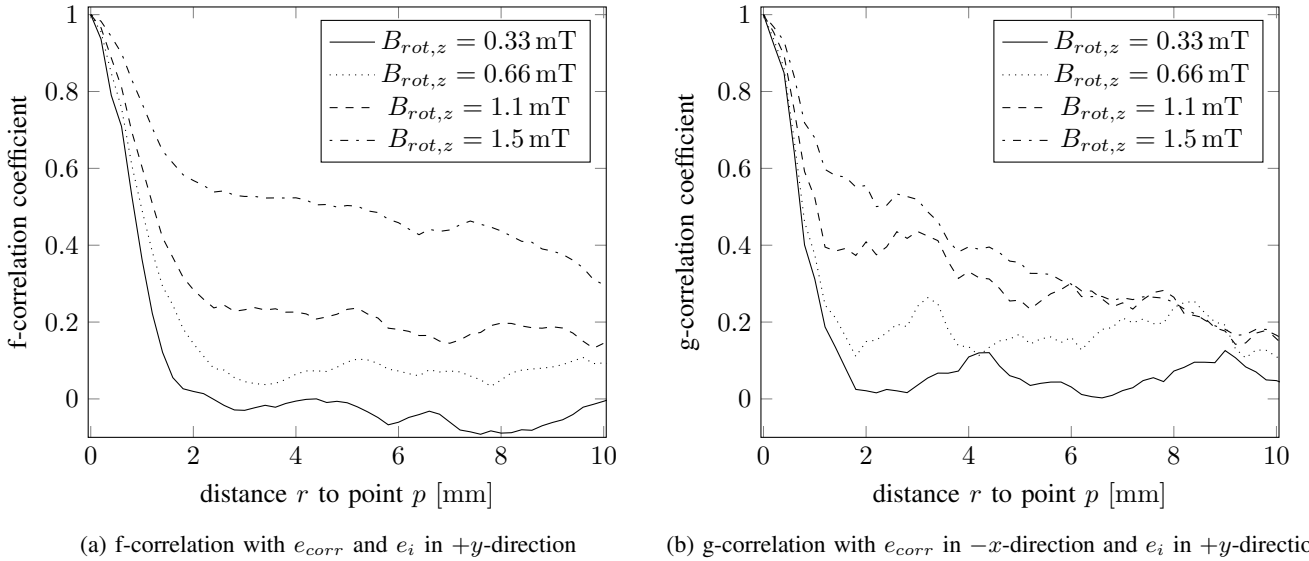


Fig. 9: Two-point correlation functions with starting point at  $p = (31 \text{ mm}, 0, 0)$ : f-correlation (a) and g-correlation (b) with the  $y$  velocity component

in the field of MHD and to flow investigations of redox flow batteries based on zinc-electrolyte slurries.

#### ACKNOWLEDGEMENT

The authors like to thank Dirk Rübiger and Sven Franke from the Helmholtz-Zentrum Dresden-Rossendorf (HZDR) for providing the experimental setup. Furthermore, we like to thank the Deutsche Forschungsgemeinschaft (DFG) for funding the project within the grant DFG BU 2241/2-1.

#### REFERENCES

- [1] K. Okazawa, T. Toh, J. Fukuda, T. Kawase, M. Toki, "Fluid Flow in a Continuous Casting Mold Driven by Linear Induction Motors," in *ISIJ International*, vol. 41, no. 8, pp. 851–858, 2001.
- [2] K. Dadzis, K. Niemietz, O. Pätzold, U. Wunderwald, and J. Friedrich, "Non-isothermal model experiments and numerical simulations for directional solidification of multicrystalline silicon in a traveling magnetic field," *Journal of Crystal Growth*, vol. 372, pp. 145–156, 2013.
- [3] L. Feierabend, S. Burgmann, B. Oberschachtsiek, and A. Heinzl, "Flow modeling of zinc-electrolyte slurries for hydraulically rechargeable zinc-air batteries," in *11th Symposium for Fuel Cell and Battery Modeling and Experimental Validation*, Winterthur, Switzerland, March 2014.
- [4] S. Eckert, G. Gerbeth, D. Rübiger, B. Willers, and C. Zhang, "Experimental modeling using low melting point metallic melts: Relevance for metallurgical engineering," *Steel Res. Int.*, pp. 419–425, 2007.
- [5] Y. Takeda, "Development of an ultrasound velocity profile monitor," *Nucl. Eng. Des.*, vol. 126, no. 2, pp. 277 – 284, 1991.
- [6] R. Nauber, M. Burger, L. Büttner, S. Franke, D. Rübiger, S. Eckert, and J. Czarske, "Novel ultrasound array measurement system for flow mapping of complex liquid metal flows," *The European Physical Journal Special Topics*, vol. 220, no. 1, pp. 43–52, 2013.

- [7] R. Nauber, M. Burger, M. Neumann, L. Büttner, K. Dadzis, K. Niemietz, O. Pätzold, and J. Czarske, "Dual-plane flow mapping in a liquid-metal model experiment with a square melt in a traveling magnetic field," *Experiments in Fluids*, vol. 54, no. 4, pp. 1–11, 2013.
- [8] V. Schmitz, W. Müller, and G. Schäfer, "Synthetic aperture focussing technique: State of the art," in *Acoustical Imaging*, ser. Acoustical Imaging, H. Ermert and H.-P. Harjes, Eds. Springer US, 1992, vol. 19, pp. 545–551.
- [9] G. van Rossum and F. Drake, *Python Reference Manual*, PythonLabs, Virginia, USA, 2001. [Online]. Available: <http://www.python.org>
- [10] M. Molero-Armenta, U. Iturrarn-Viveros, S. Aparicio, and M. Hernández, "Optimized opencl implementation of the elastodynamic finite integration technique for viscoelastic media," *Computer Physics Communications*, vol. 185, no. 10, pp. 2683 – 2696, 2014.
- [11] A. Klöckner, N. Pinto, Y. Lee, B. Catanzaro, P. Ivanov and A. Fasih, "PyCUDA and PyOpenCL: A Scripting-Based Approach to GPU Run-Time Code Generation," *ArXiv e-prints*, 0911.3456, 2009.
- [12] C. Kasai, K. Namekawa, A. Koyano, and R. Omoto, "Real-time two-dimensional blood flow imaging using an autocorrelation technique," *IEEE Transactions on Sonics and Ultrasonics*, vol. 32, no. 3, pp. 458 – 464, 1985.
- [13] A. Jensen, "Estimation of blood velocities using ultrasound: a signal processing approach," *Cambridge University Press*, 1996.
- [14] P. J. Phillips, A. P. Kadi, and O. T. von Ramm, "Feasibility study for a two-dimensional diagnostic ultrasound velocity mapping system," *Ultrasound in medicine & biology*, vol. 21, no. 2, pp. 217–229, 1995.
- [15] A. Pastorelli, G. Torricelli, M. Scabia, E. Biagi and L. Masotti, "A Real-Time 2-D Vector Doppler System for Clinical Experimentation," *IEEE Transactions on Medical Imaging*, vol. 27, no. 10, pp. 1515-1524, 2008
- [16] A. Jensen, I. Nikolov, A. Yu, D. Garcia, "Ultrasound Vector Flow Imaging Part II: Parallel Systems," *IEEE Transactions on Ultrasonics, Ferroelectrics and Frequency Control*, vol. 63, no. 11, pp. 1722–1732, 2016.
- [17] I. Grants and G. Gerbeth, "Stability of axially symmetric flow driven by a rotating magnetic field in a cylindrical cavity," *J. Fluid Mech.* vol. 431, pp. 407 – 426, 2001.
- [18] L. Büttner, R. Nauber, M. Burger, D. Rübiger, S. Franke, S. Eckert and J. Czarske, "Dual-plane ultrasound flow measurements in liquid metals," *Meas. Sci. and Technol.*, vol. 24, 2013.
- [19] P. A. Davidson and J. C. R. Hunt, "Swirling recirculation flow in a liquid-metal column generated by a rotating magnetic field," *Journal of Fluid Mechanics*, vol. 185, pp. 67 – 106, 1987.
- [20] K. Fraña and J. Stiller, "A numerical study of flows driven by a rotating magnetic field in a square container," *European Journal of Mechanics - B/Fluids*, vol. 27, no. 4, pp. 491 – 500, 2008.
- [21] OpenCFD, "OpenFOAM - The Open Source CFD Toolbox - Users Guide," *OpenCFD Ltd., United Kingdom*, 3rd ed., 2015.
- [22] R. Nauber, H. Beyer, K. Mäder, C. Kupsch, N. Thieme, L. Büttner and J. Czarske, "Modular Ultrasound Velocimeter for Adaptive Flow Mapping in Liquid Metals," in *IEEE International Ultrasonics Symposium*, Tours, France, 18 – 21 Sep 2016, 2016, entry 5K-4
- [23] P. A. Davidson, "Turbulence : an introduction for scientists and engineers," *Oxford University Press*, 2. edition, 2015.